

# Automatika

Journal for Control, Measurement, Electronics, Computing and Communications



ISSN: (Print) (Online) Journal homepage: [www.tandfonline.com/journals/taut20](http://www.tandfonline.com/journals/taut20)

## Design and Implementation of Fuzzy sliding mode control (FSMC) approach for a Modified Negative Output Luo DC-DC Converter with its comparative analysis

V. Chamundeeswari & R. Seyezhai

To cite this article: V. Chamundeeswari & R. Seyezhai (2024) Design and Implementation of Fuzzy sliding mode control (FSMC) approach for a Modified Negative Output Luo DC-DC Converter with its comparative analysis, *Automatika*, 65:1, 45-57, DOI: 10.1080/00051144.2023.2280875

To link to this article: <https://doi.org/10.1080/00051144.2023.2280875>



© 2023 The Author(s). Published by Informa UK Limited, trading as Taylor & Francis Group.



Published online: 21 Nov 2023.



Submit your article to this journal [↗](#)



Article views: 374



View related articles [↗](#)



View Crossmark data [↗](#)



# Design and Implementation of Fuzzy sliding mode control (FSMC) approach for a Modified Negative Output Luo DC-DC Converter with its comparative analysis

V. Chamundeeswari<sup>a</sup> and R. Seyezhai<sup>b</sup>

<sup>a</sup>Department of Electrical and Electronics Engineering, St. Joseph's College of Engineering, Chennai, India; <sup>b</sup>Department of Electrical and Electronics Engineering, Sri Sivasubramaniya Nadar College of Engineering, Chennai, India

## ABSTRACT

Switching power converters bring a desired output magnitude using semiconductor devices. These switching converters are generally classified as voltage lift and super lift. The conventional lift converters such as buck, boost and buck–boost come under the category of voltage lift technique, in which the output voltage increases in arithmetic progression. The other lift approach that increases the output voltage in the geometric progression is the super-lift method. Nowadays super-lift converters find their role in various applications, because of their high gain and low ripple. The converter taken for analysis is a modified negative output super-lift Luo converter (MNOSLC). Current mode control (CMC) is employed to maintain a stable DC voltage at the load side. This is investigated using different types of controllers such as PI, fuzzy, sliding mode controller (SMC) and fuzzy SMC. The performance of these controllers is compared and it is found that fuzzy SMC results in better line and load regulation. A prototype is developed that validates the simulation results.

## ARTICLE HISTORY

Received 21 August 2023  
Accepted 27 October 2023

## KEYWORDS

DC–DC converter; MNOSLC; ripple; fuzzy; SMC

## 1. Introduction



MNOSLC is a type of super-lift converter which produces a very high negative voltage with low ripple. It is derived from the conventional NOSLC circuit. The modified topology is formed by adding an inductor  $L_2$  and diode  $D_3$  to the elementary NOSLC circuit. The negative converter is preferred because negative voltage prevents corrosion in metals, reduces the effect of lightning in telecom towers, overcomes wet cable problems, aids in cathodic protection and helps in the long-distance transmission of signals.

The proposed topology shows an increase in voltage transfer ratio with the increase in passive energy storage components. The increase in gain is mainly achieved by the inductor and diode–capacitor multiplier combination in the circuit. One more significant advantage is the presence of only one switching device which overcomes the effect of switching loss and conduction loss.

Although MNOSLC is a new topology, it is always desirable to have regulation at the line and load side, which is mandatory for any DC–DC converter. Here, the technique adopted for line regulation is the current mode control (CMC). This control [1] provides an effective closed-loop performance and makes the circuit produce the desired output in every region of operation. DC–DC converters are generally employed

with voltage mode control in which the output voltage is taken as a feedback signal. However, this control will not provide an appropriate control action under different operating conditions. So, an additional loop referred to as the current loop is implemented that resolves the problem of voltage mode control. The interrelation between the voltage and current mode lies in generating the current reference. The influence of potential change in voltage mode control is compensated by the current loop introduced that provides a reference signal [2] for loop regulation. CMC also offers a good dynamic performance regardless of the operating conditions.

The analysis of CMC is carried out in a detailed way using various controllers in this research. These controllers have been modelled and employed to generate the current reference for good voltage regulation in the circuit. The controllers employed are Proportional–Integral (PI) controller [3], fuzzy [4], Sliding mode controller (SMC) [5] and fuzzy SMC (FSMC) [6]. The characteristics of each and every controller are analysed for different operating points and its response curves are plotted. Since the dynamic response is found better with low ripple characteristics in FSMC compared to the other controllers, FSMC is chosen for the current mode control to achieve better regulation.

**CONTACT** V. Chamundeeswari  [chamuvins@gmail.com](mailto:chamuvins@gmail.com)  Department of Electrical and Electronics Engineering, St. Joseph's College of Engineering, Chennai 600119, India

This article has been corrected with minor changes. These changes do not impact the academic content of the article.

© 2023 The Author(s). Published by Informa UK Limited, trading as Taylor & Francis Group.

This is an Open Access article distributed under the terms of the Creative Commons Attribution License (<http://creativecommons.org/licenses/by/4.0/>), which permits unrestricted use, distribution, and reproduction in any medium, provided the original work is properly cited. The terms on which this article has been published allow the posting of the Accepted Manuscript in a repository by the author(s) or with their consent.

Another important factor that led to the choice of FSMC is the reduced chattering level in its time-varying response. Thus, the FSMC technique provides an inner current loop control with the aid of an outer voltage loop.

Section 2 deals with an overview of the proposed work and the modes of operation of MNOSLC. Section 3 deals with the modelling of MNOSLC. Section 4 deals with current mode control and its implementation using conventional controllers. Section 5 deals with current mode control implementation using FSMC along with its prototype developed for line and load regulation. Finally, Section 6 ends with a conclusion.

## 2. Overview of the proposed work

The topological structure includes only an additional inductor and diode in the conventional NOSLC to form MNOSLC. The output voltage increases in geometric progression and it is almost six times the input voltage which is drastically high. Thus, a power-efficient DC–DC converter is portrayed in the proposed work.

This section describes the working of a modified Luo converter with its modes of operation and equations [7]. The analysis of this novel DC–DC Converter with its simulation waveforms and a prototype developed has also been clearly depicted. A slight change in the topological structure of NOSLC brings high gain and reduced ripple in its output voltage. The gain of the proposed MNOSLC is found three times higher than the conventional NOSLC circuit. The performance parameters also reveal that the proposed is better compared to the conventional circuit.

### 2.1. Modes of operation

Figure 1 shows the circuit of MNOSLC. It consists of DC supply voltage  $V_1$ , capacitors  $C_1$  and  $C_2$ , inductor  $L_1$  and  $L_2$ , switch  $S_1$ , diodes  $D_1, D_2, D_3$  and a load resistance  $R_1$ . The working principle is explained with the switch “ $S_1$ ” on and off in two modes of operation, as shown in Figures 2 and 3.

In mode 1, the switch  $S_1$  is turned on between the period 0 and  $\Delta T$ . When the switch is closed, the source voltage causes the current to flow through inductor  $L_1$  and capacitor  $C_2$ . Since capacitor  $C_2$  has zero impedance to current, capacitor  $C_2$  charges faster than

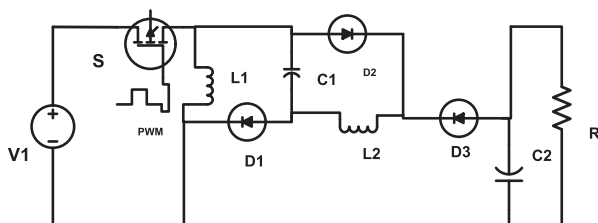


Figure 1. Circuit diagram of Topology 3: MNOSLC.

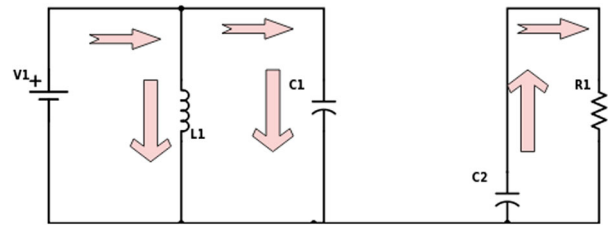


Figure 2. Circuit diagram of mode 1.

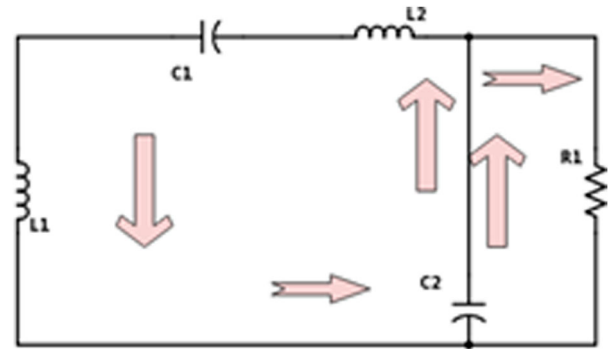


Figure 3. Circuit diagram of mode 2.

inductor thus forward biasing the diode  $D_1$ . Thus, the charge gets stored in inductors  $L_1, L_2$  and capacitor  $C_2$ . During this period, the load current is maintained constant by the discharging capacitor  $C_1$ . Thus the energy stored in the capacitor  $C_1$  during the previous cycle is transferred to the load.

In mode 2, the switch  $S_1$  is turned off between the period  $\Delta T$  and  $T$ . In this mode, when the switch is open, the energy that is stored in the inductors  $L_1, L_2$  and the capacitor  $C_1$  discharge across the nodal points of the capacitor  $C_2$ , thus boosting the output voltage. To include figures, tables or text in mode 2, the switch  $S_1$  is turned off between the period  $\Delta T$  and  $T$ . In this mode, when the switch is open, the energy that is stored in the inductors  $L_1, L_2$  and the capacitor  $C_1$  discharge across the nodal points of the capacitor  $C_2$ , thus boosting the output voltage.

## 3. Modelling of MNOSLC

The equations governing mode 1 are as follows.

The input voltage  $V_1$  is given in terms of current flow through the inductor

$$V_1 = L_1 \frac{di_i}{dt} \tag{1}$$

$V_1$  can also be represented as

$$V_{C_1} = V_1 \tag{2}$$

where  $V_{C_1}$  is the voltage across the capacitor  $C_1$ .

The current through the inductor  $L_1$  is given by

$$I_{L_1} = \frac{V_{in} dt}{L_1} = \frac{V_{in} k T}{L_1} \tag{3}$$

where  $k$  is the duty ratio and  $T$  is the on-period cycle.

**Table 1.** Simulation parameters of MNOSLC.

| Parameters                      | Values                 |
|---------------------------------|------------------------|
| $V_{in}$ (input voltage)        | 6 V                    |
| $f_s$ (switching frequency)     | 50 kHz                 |
| $k$ (duty ratio)                | 0.67                   |
| $R$ (resistive load)            | 100 $\Omega$           |
| Expected $V_0$ (output voltage) | -36.36 V               |
| $L_1, L_2$ (inductors)          | 0.01 Mh                |
| $C_1, C_2$ (capacitors)         | 30 $\mu$ F, 10 $\mu$ F |

The voltage across the capacitor  $C_2$  is the load or the output voltage  $V_0$  and during mode 1 it is given as

$$V_{C_2} = V_0 \quad (4)$$

The current through the capacitor  $C_2$  during on is given by

$$I_{C_{2on}} = I_0 = C_2 \frac{dv_0}{dt} \quad (5)$$

During mode 2, the current through the inductor  $L_1$  is given by

$$I_{L_1} = \frac{V_0 - V_{in}}{L_1} dt = \frac{V_0 - V_{in}}{L_1} (1 - k) T \quad (6)$$

where  $V_0$  is the output voltage and  $(1 - k) T$  is the off-period cycle.

The current through the inductor  $L_2$  is given by

$$I_{L_2} = \frac{V_0 - V_{in}}{L_2} dt = \frac{V_0 - V_{in}}{L_2} (1 - k) T \quad (7)$$

Equating (3) and (6),

$$\frac{V_{in} k T}{L_1} = \frac{V_0 - V_{in}}{L_1} (1 - k) T \quad (8)$$

From the above, the gain equation is obtained as

$$\frac{V_0}{V_{in}} = \frac{2}{1 - k} \quad (9)$$

The output voltage is given by

$$V_0 = \frac{2V_{in}}{1 - k} \quad (10)$$

Using the design equations, the simulation parameters are computed, as shown in Table 1.

### 3.1. Simulation results

MNOSLC is simulated using the design values and the results are shown in Figure 4.

Figure 4 depicts the simulation results of MNOSLC. For an input voltage of 6 V, as shown in Figure 4(a), the output voltage obtained is -36.36 V as shown in Figure 4(b). Figure 4(c,d) represents the input current as 2.337 A and the output current as -0.36 A. The voltage across the diode  $D_2$  is shown as 38 V in Figure 4(e,f) show the voltage across the diode  $D_3$  as 44 V. Figure 4(g,h) represents the voltage across capacitor  $C_1$  and the current through the inductor  $L_1$  as 5.1 V and 2.54 A, respectively.

## 4. Current mode control

Generally, voltage regulation is achieved by employing a suitable controller in DC-DC converters. The controller employed for DC regulation in the referred MNOSLC is the current mode control (CMC). In this

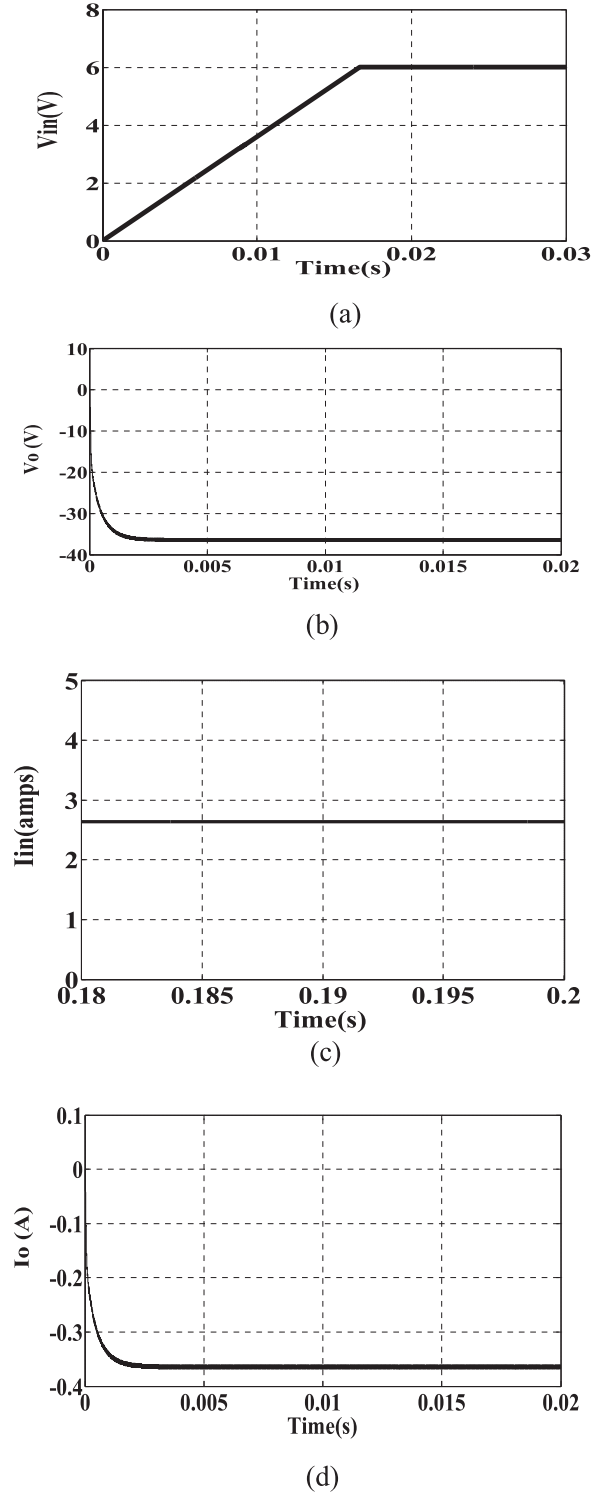


**Figure 4.** Waveforms of MNOSLC. (a) Input voltage of 6 V, (b) output voltage of -36.36 V, (c) input current of 2.637 A, (d) output current of -0.36 A, (e) voltage across the diode  $D_2 = 38$  V, (f) voltage across the diode  $D_3 = 44$  V, (g) voltage across the capacitor  $C_1$  as 5.1 V and (h) current through the inductor  $L_1$  as -2.54 A.

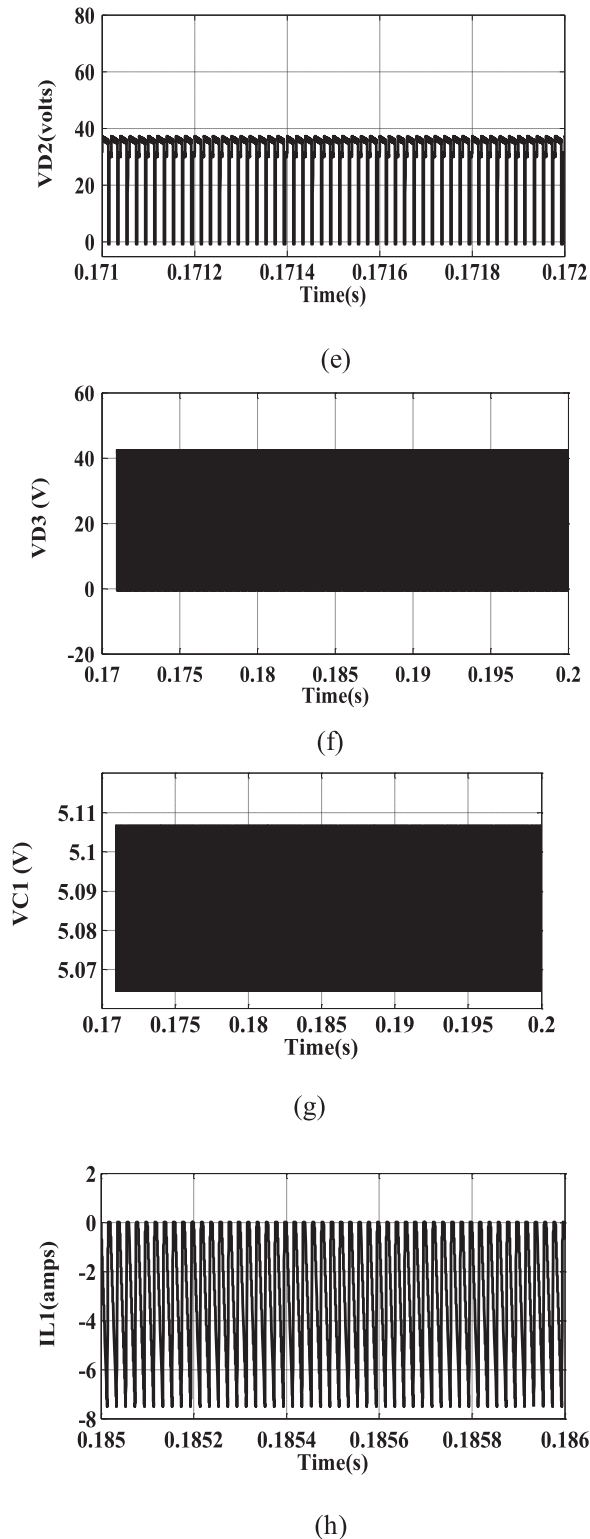


Figure 4. Continued

technique, [8] the control signal is generated through the inner current loop. However, it is indirectly influenced by the outer voltage loop. The two control loops are effectively involved in this CMC technique. First, in the voltage loop, the output voltage of MNOSLC is sensed and compared with the reference signal to generate the error voltage. This is compared with a ramp-like inductor current to generate the desired PWM signal. Thus, the outer loop provides a correct control

reference for the inner loop [9]. The comparator outputs a latching signal for the switch to turn on and off.

With this concept, several linear and non-linear controllers are investigated in this chapter. A controller generally modifies the error signal and produces a proper control to get the desired output. The controllers employed for MNOSLC compensate for the load variations and give stabilized output from the DC-DC converter. To have a mandatory closed-loop regulation of the DC-DC converter, the controllers employed are Proportional-integral (PI), fuzzy PI, Sliding mode controller (SMC) [10] and fuzzy SMC. Since PI acts as a linear controller, compensation for the nonlinearities is introduced using fuzzy [11] and sliding mode controllers. Although fuzzy and SMC showed a good dynamic approach, they show sluggish responses. To overcome this, an integrative method is employed by combining fuzzy and SMC as FSMC [12]. This gives a better dynamic response and generates the exact reference signal for the inner CMC technique [13].

#### 4.1. Description of controllers

To achieve voltage regulation, the PI controller, fuzzy, sliding mode controller and fuzzy sliding mode controller are studied. These controllers are verified and their characteristic outputs are depicted from which the proposed controller is chosen.

First, a PI controller is designed and implemented for MNOSLC [14].  $K_p$  and  $T_i$  are the PI parameters, which are tuned using Ziegler-Nichols tuning [15] and used in the transfer function of the controller and it is simulated. Although the controller proves to be a better linear controller it may not respond well to changes in the operating point. To overcome this, a non-linear controller, namely a fuzzy controller is designed by fuzzyfying the  $K_p$  and  $T_i$  values [16] with expert knowledge. Here, it works only for a systematic approach and prefers the trial and error method in the absence of expert understanding. So, a robust method of control is implemented using SMC for uncertainties and other disturbances. Although the output voltage reaches its desired value in this, the ripple is higher than the other two control techniques. Considering the noteworthy features of fuzzy and SMC a combinational controller, named fuzzy SMC (FSMC) [17,18], is developed and proposed here. The proposed approach showed a better characteristic output and also a satisfactory operation in all regions. The generation of reference magnitude is carried out by the prescribed FSMC method in the current mode control [19].

##### 4.1.1. Implementation of PI controller for MNOSLC

This section deals with the PI controller. The PI controller modifies the error signal and produces a

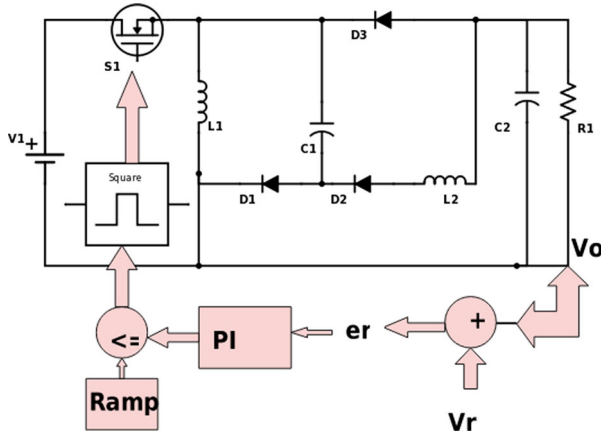


Figure 5. PI controller for MNOSLC.

proper output. Initially, the converter transfer function is calculated and the step response is obtained. From the response curve, the proportional constant  $K_p$  and the integral constant  $T_i$  values are estimated using Ziegler–Nichols tuning. These values of  $K_p$  and  $T_i$  are then used for predicting the transfer function of the controller.

The transfer function of the controller is given as

$$\frac{V_o(s)}{V_i(s)} = \frac{s + 1.174e - 14}{s} \quad (11)$$

Thus, the design of the controller using the transfer function decides the reference magnitude of the control signal.

Figure 5 shows the PI controller implemented for MNOSLC [20]. Here, the output voltage is measured and compared with its reference signal “C”. The error generated is given to the controller transfer function block “TF”. The controller modifies the error signal and produces a proper latching signal to the switch “S<sub>1</sub>” by comparing it with a repeating sequence ramp signal.

The simulation results of MNOSLC using a PI controller are depicted in Figure 6(a–f). Figure 6(a) shows the input voltage of 6 V and the output voltage of  $-34.69$  V as depicted in Figure 6(b). The input current of 2.7 A is shown in Figure 6(c) and the corresponding output current of  $-0.35$  A is shown in Figure 6(d). Since there are two capacitors, the voltage across the capacitor  $C_1$  is shown in Figure 6(e) as 5.1 V and the diode voltages  $D_2$  and  $D_3$  are represented in Figure 6(f,g) as 36 and 41 V, respectively.

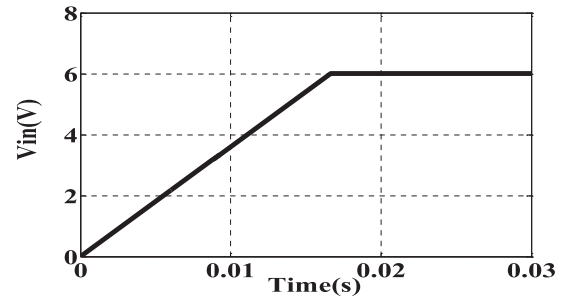
#### 4.1.2. Analysis of output voltage ripple in the MNOSLC-fed PI controller

The ripple waveform of about 1.57% is shown in Figure 7. The maximum and minimum magnitude of the signal is  $-34.7$  and  $-35.25$  V, respectively.

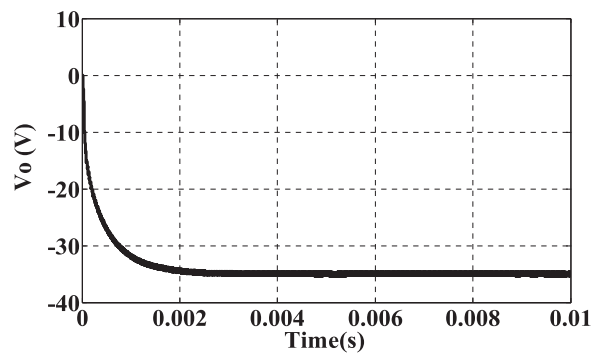
It shows the ripple obtained in the closed loop of MNOSLC with the PI controller which is low when compared to the ripple in the open loop value of 1.64%.

#### 4.1.3. Implementation of fuzzy controller for MNOSLC

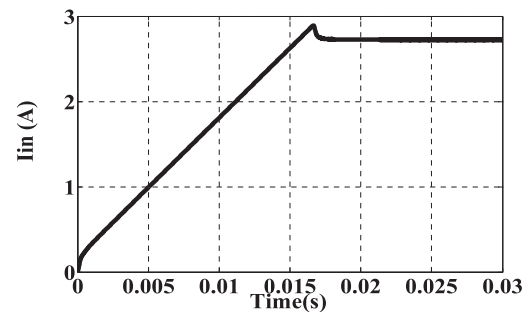
The PI controller is a good linear controller but may not respond well to non-linear conditions. Hence fuzzyfying the values of  $K_p$  and  $T_i$  [21] using expert



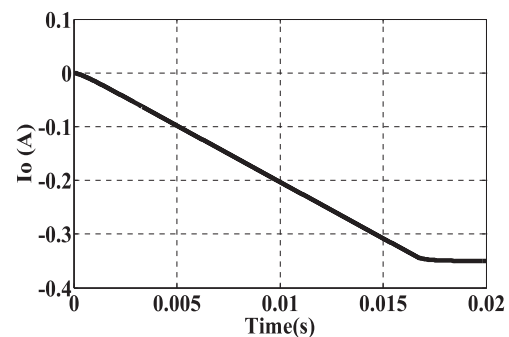
(a)  $V_{in} = 6$  V



(b)  $V_o = -34.69$  V



(c)  $I_{in} = 2.7$  A



(d)  $I_o = -0.35$  A

Figure 6. Waveforms of MNOSLC using the PI controller. (a) Input voltage of 6 V, (b) output voltage of  $-34.69$  V, (c) input current of 2.7 A, (d) output current of  $-0.35$  A, (e) voltage across the capacitor  $C_1$  of 5.1 V, (f) voltage across the diode  $D_2$  of 36 V and (g) voltage across the diode  $D_3$  of 41 V.

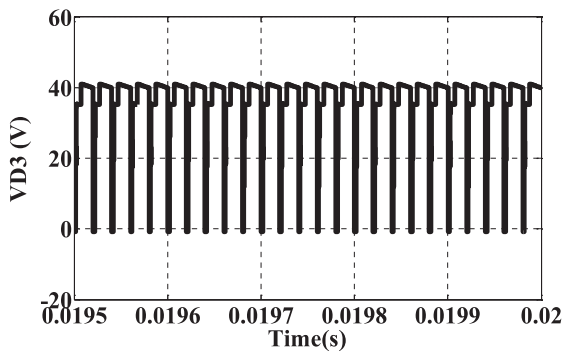
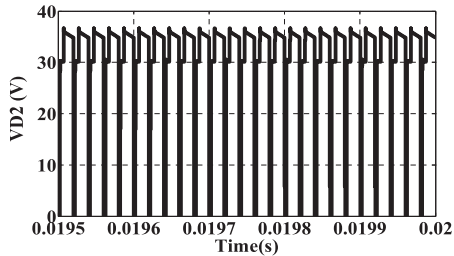
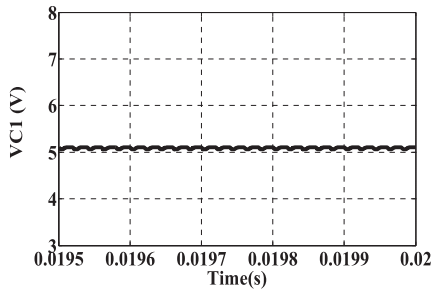


Figure 6. Continued

understanding of the system makes it act as a very good non-linear controller [22].

In the fuzzy controller [23], as shown in Figure 8, the output voltage is taken and compared with the reference. The error generated is given to the fuzzy controller. Since the fuzzy is a systematic approach controller [24], it generates the latching signal for the

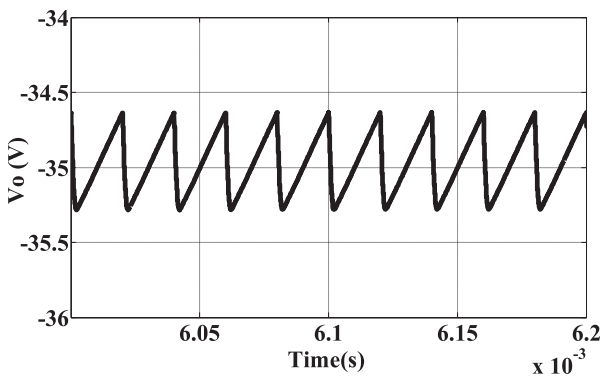


Figure 7. Output voltage ripple waveform – PI controller.

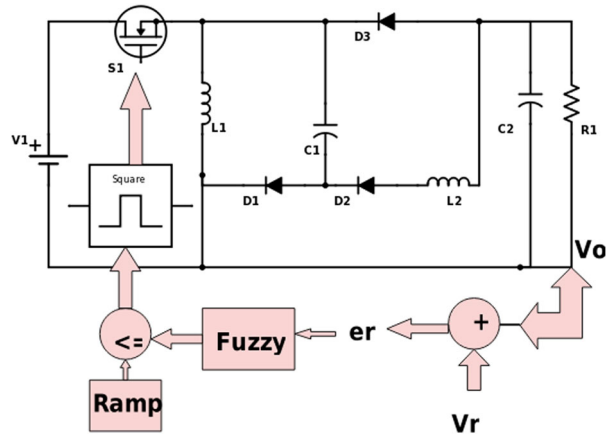


Figure 8. Fuzzy controller for MNOSLC.

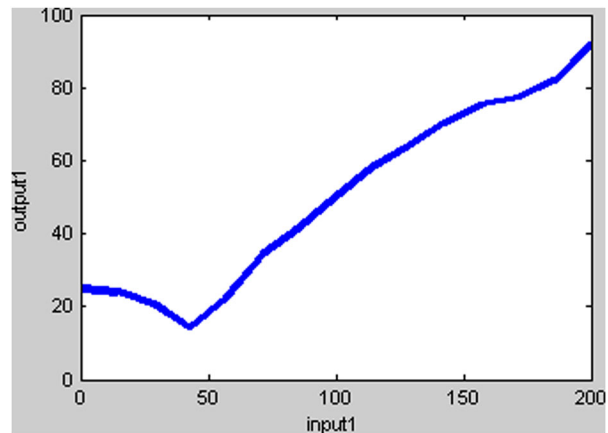


Figure 9. Fuzzy surface viewer.

switch “ $S_1$ ” with its knowledge-base rule. The surface viewer with its knowledge base is given in Figure 9.

Figure 9 shows the surface viewer of MNOSLC in a fuzzy controller. The input in the plot represents the error signal from the comparator given to the controller and the output is the reference control magnitude generated from the fuzzy controller. This signal is again compared with the ramp to generate the switching pulse for the converter.

The fuzzy expert knowledge [25] works only on the rule base and the rules are tabulated in Table 2.

Table 2 conveys the relation between the input fed to the fuzzy controller and the output obtained from the fuzzy block. It has segregated the error magnitude as negative (N), small (S), zero (Z), positive (P) and positive big (PB). It has been denoted that if the error

Table 2. Rule base table for a fuzzy controller.

| Error (e) | Duty ratio (D) |
|-----------|----------------|
| S         | VS             |
| NS        | S              |
| Z         | M              |
| P         | L              |
| PB        | VL             |

is small, the latching magnitude should be very small and for a very small value of error which is called a negative small, the duty ratio should be small magnitude. In the same way, the rules have been framed for the larger values of error with their corresponding duty ratio magnitudes.

#### 4.1.4. Simulation results of fuzzy controller

The simulation results are depicted for fuzzy controller-based MNOSLC in Figure 10(a–f). It shows the input voltage of 6 V in Figure 10(a) and the output voltage of  $-35.5$  V in Figure 10(b). For an input current of 2.7 A, the output current of  $-0.36$  A is obtained as shown in Figure 10(c,d). The voltage across the capacitor  $C_1$  is 6 V in Figure 10(e).

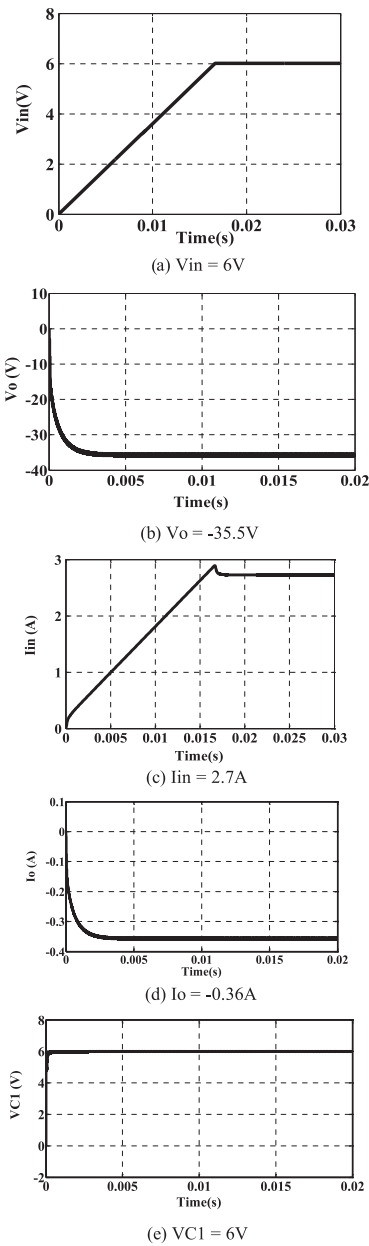


**Figure 10.** Waveforms of MNOSLC using a fuzzy controller. (a) Input voltage of 6 V, (b) output voltage of  $-35.5$  V, (c) input current of 2.7 A, (d) output current of  $-0.36$  A and (e) voltage across the capacitor  $C_1$  of 6 V.

#### 4.1.5. Analysis of output voltage ripple in the MNOSLC-fed fuzzy controller

The ripple waveform of about 1.15% is shown in Figure 11. The maximum and minimum magnitude of the signal is  $-35.42$  and  $-35.83$  V, respectively.

#### 4.1.6. Implementation of the sliding mode controller for MNOSLC

Controllers like PI and fuzzy have been verified for the proposed MNOSLC circuit. PI has shown its result with the justified proportional and integral constant values and fuzzy has shown itself as a controller that works based on expert knowledge and systematic understanding. Since it is a knowledge-based approach, it has made its effort with the trial and error method which sometimes is a time-consuming approach. Having these uncertainties, SMC is predicted which works on the concept of sliding coefficient selection. One significant feature of SMC is that the error magnitude generation is not only from the load side but also it considers signal from the line side capacitor and inductor [26]. It senses the values of those elements and compares them with the respective reference signal to generate the latching signal of switch  $S_1$ .

#### 4.1.7. Analysis of SMC

A sliding surface equation in the state space can be expressed by a linear combination of state-variable errors as given by

$$S = (i_{L1}, V_{C1}, V_{C2}) = K_1 \varepsilon_1 + K_2 \varepsilon_2 + K_3 \varepsilon_3 \quad (12)$$

where coefficients  $K_1$ ,  $K_2$  and  $K_3$  are proper gains,  $\xi_1$  is the feedback current error,  $\xi_2$  is the feedback voltage error and  $\xi_3$  is the feedback voltage error.

$$\varepsilon_1 = i_{L1} - i_{L1ref} \quad (13)$$

$$\varepsilon_2 = V_{C1} - V_{C1ref} \quad (14)$$

$$\varepsilon_3 = V_{C2} - V_{C2ref} \quad (15)$$

By substituting (13), (14) and (15) in (12) the sliding surface “S” equation is obtained as

$$S = (i_{L1}, V_{C1}, V_{C2}) = K_1 (i_{L1} - i_{L1ref}) + K_2 (V_{C1} - V_{C1ref}) + K_3 (V_{C2} - V_{C2ref}) \quad (16)$$

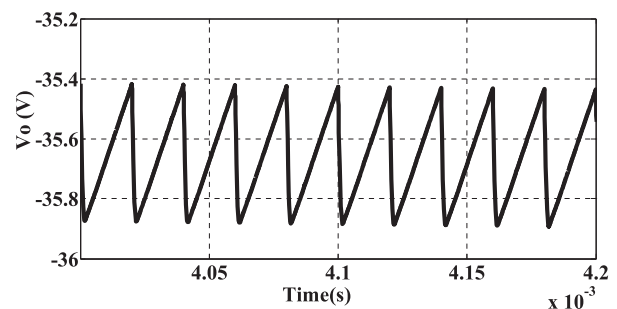


**Figure 11.** Output voltage ripple waveform – fuzzy controller.



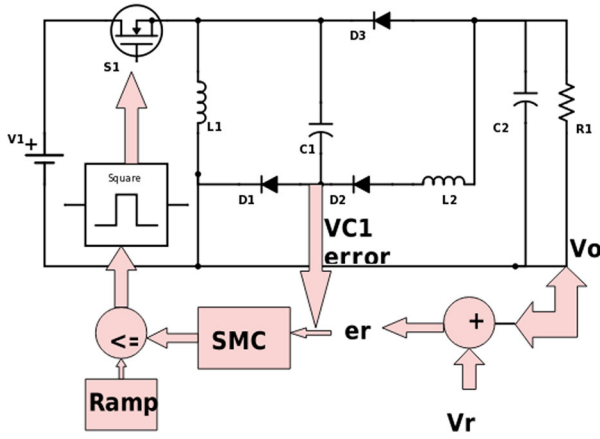


Figure 12. Sliding mode controller for MNOSLC.

Thus, the sliding surface equation obtained in (16) reflects that it is dependent on the error generated by the passive component signals. This error magnitude given as an input to SMC [27] is rectified and a proper latching signal is provided to the converter.

Figure 12 portrays the SMC controller implemented for MNOSLC. The inductor current and the capacitor voltages are measured and compared with its references multiplied by its gain parameters and then fed to the adder. The output of the adder is then compared with a ramp signal to generate the control magnitude for the switch  $S_1$  of the converter.

4.1.8. Simulation results of SMC

The simulation results are depicted for SMC in this section.

Figure 13(a–e) portrays the outputs obtained. Figure 13(a) represents the input voltage of 6 V and the respective input current of  $-4.2$  A as shown in Figure 13(b). Figure 13(c) shows the output voltage and output current of  $-35.75$  V and  $-0.50$  A, respectively. The voltage across the capacitor  $C_1$  is 5 V in Figure 13(d,e) represents the voltage across the diode of 42 V.

4.1.9. Analysis of output voltage ripple in MNOSLC-fed SMC

The ripple analysis is carried out for the output voltage in SMC control. Figure 14 represents the ripple waveform of output voltage.

The maximum and minimum magnitude level is  $-35.25$  and  $-36.88$  V, respectively. Here the ripple is 4.51%. Although the ripple is slightly high, SMC has produced the required high magnitude output than the conventional PI and fuzzy and the settling time of the response is 0.0005 s which is faster than that of the conventional controllers.

Chattering is defined as the oscillations in the control output that result in instability. SMC technique introduces this kind of chattering which is overcome in fuzzy-based SMC. Tuning the rule base of fuzzy makes the system travel on the sliding surface “S” in the FSMC technique and provides stability to the system.

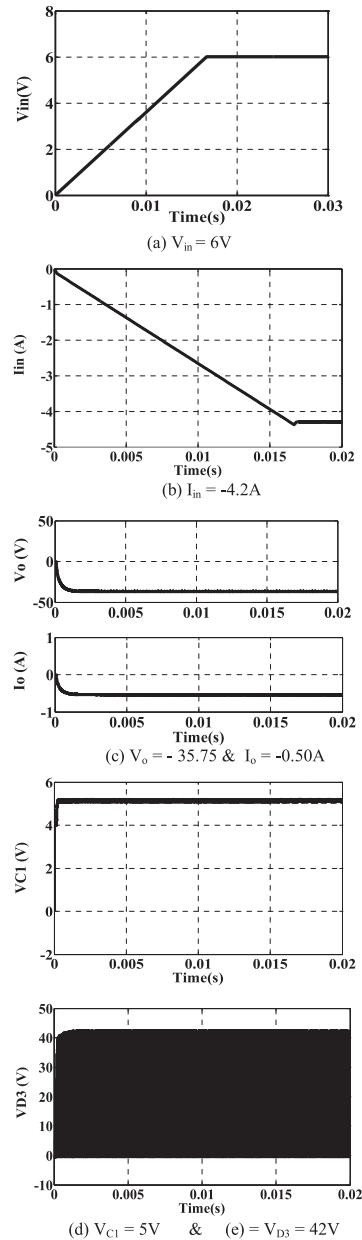


Figure 13. Waveforms of MNOSLC using a sliding mode controller. (a) Input voltage of 6 V, (b) input current of  $-4.2$  A, (c) output voltage of  $-35.75$  V, output current of  $-0.50$  A, (d) voltage across the capacitor  $C_1$  of 5 V and (e) voltage across the diode  $D_3 = 42$  V.

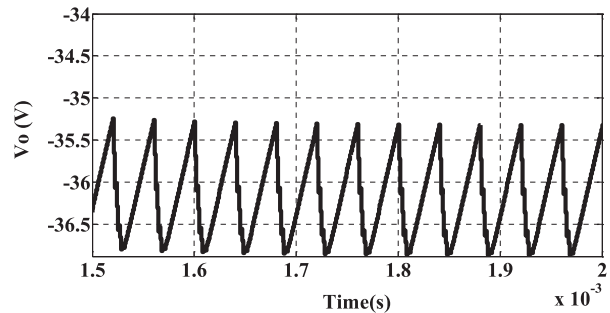


Figure 14. Output voltage ripple waveform – SMC.

When ripple is more, it provides an unregulated DC output in converters and also discontinuous conduction. Chattering results in low control accuracy and heat

**Table 3.** Comparative analysis of PI, fuzzy and SMC.

| Parameter                    | PI     | Fuzzy   | SMC     |
|------------------------------|--------|---------|---------|
| Output voltage ( $V_o$ in V) | -34.69 | -35.5   | -35.75  |
| Settling time ( $t_s$ in s)  | 0.0018 | 0.004 s | 0.003 s |
| Ripple (in %)                | 1.57   | 1.15    | 4.51    |

losses in electric circuits. It is caused due to unmodelled dynamics and discrete time implementation which lowers the accuracy of the control. Chattering is created because of sliding mode control.

#### 4.2. Comparative analysis of PI, fuzzy and SMC

The analysis of the controllers is tabulated in Table 3.

It has conveyed the feature of SMC in its output voltage of  $-35.75$  V, which is slightly higher than the conventional PI and fuzzy whose values are  $-34.69$  and  $-35.5$  V, respectively. The time domain characteristics have also shown SMC as a better controller since the response of SMC settles at a sooner time of  $0.003$  s [28] than the PI and fuzzy whose settling time values are  $0.0018$  and  $0.004$  s, respectively. It has revealed the feature of fuzzy in its ripple reduction though it is a slow expert-based approach. Having these features, named FSMC is developed in this work to meet the uncertainties and produce a steady-state output.

### 5. Implementation of FSMC with CMC for MNOSLC

The proposed controller [29] overcomes the phenomenon of chattering, reduces the settling time and provides a good dynamic response compared to classical controllers such as PI, fuzzy and SMC.

The FSMC [30] is explained with the concept of fuzzyfying SMC parameters using a stability approach. It defines a sliding surface "S" [31] and the reach of the surface is highly obtained with the rule frame technique in fuzzy. The rule frame logic brings control in the duty ratio "D" of the switching pulse of the converter, thereby maintaining steady-state output. The FSMC satisfies the condition of Lyapunov stability which is given by

$$S^* dS < 0 \text{ where } dS \text{ is the derivative of } S \quad (17)$$

The duty cycle increase and decrease is obtained only by  $S$  and  $dS$ .

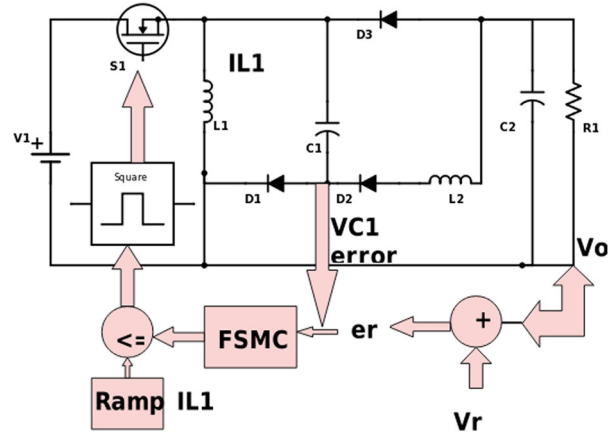
The sliding surface equation is formed only with the generated errors which are given below.

$$S = k_1 \xi_1 + k_2 \xi_2 \quad (18)$$

where  $k_1$  and  $k_2$  are the respective error gains and  $\xi_1$  and  $\xi_2$  are the errors generated from the voltages of the load and input capacitor by comparing with its references. This sliding surface and its derivative act as an input to the fuzzy block, thereby generating the required duty ratio for the converter. Thus, the fuzzy

**Table 4.** Rule table of FSMC.

| $e\Delta e$ | Z  | PS | PL |
|-------------|----|----|----|
| NL          | NL | NS | ZE |
| NS          | NS | ZE | PS |
| Z           | ZE | PL | PS |
| PS          | PS | PL | PL |
| PL          | PL | PL | PL |

**Figure 15.** Fuzzy sliding mode controller for MNOSLC.

rule table forms the controlled duty ratio for the converter. These control signals are assigned with five values negative big, negative small, zero, positive big and positive small. The change in error to the fuzzy block, one of the control signals, gives the desired duty ratio, thereby maintaining the output to a steady-state value. The rule table is tabulated in Table 4.

Figure 15 represents the FSMC control of MNOSLC [32] for current mode control. The reference for CMC [33], (Fang W, Liu X-D, Liu S-C, et al) is generated using the fuzzy sliding mode controller. To generate the reference signal, it first compares the load voltage and the voltage across the input capacitor with its standard references and generates the error signal. These error signals are multiplied with their respective gains fed to the controller and modified to produce a proper control output that acts as a reference for current mode control [34]. Thus, the outer voltage loop influences the inner current loop.

The current mode control [35] is employed. It senses the inductor current and the rise and fall ramp signal is fed to a comparator as one of the inputs and the control magnitude from FSMC is fed as the other input. Thus both are compared and the required PWM signal for the converter is produced. So, the inner loop brings a regulation in the converter with the aid of the outer loop [36].

To compensate for the non-linearities produced in other controllers, FSMC is implemented. It overcomes the drawbacks of the conventional and produces the desired steady-state output with less chattering and ripple. Since fuzzy acts as a trial-and-error-oriented method, sliding mode control is implemented that works on the concept of sliding surface "S" selection.

**Table 5.** Comparative analysis of fuzzy, SMC and Fuzzy SMC control-fed MNOSLC.

| Parameters            | Fuzzy    | SMC       | FSMC             |
|-----------------------|----------|-----------|------------------|
| $t_d$ (delay time)    | 0.0001 s | 0.00006 s | <b>0.00005 s</b> |
| $t_r$ (rise time)     | 0.001 s  | 0.0009 s  | <b>0.0001 s</b>  |
| $t_s$ (settling time) | 0.004 s  | 0.003 s   | <b>0.001 s</b>   |
| Oscillatory response  | Yes      | Yes       | <b>No</b>        |
| Ripple (%)            | 1.816    | 1.709     | <b>1.64</b>      |

The system response is made to follow the sliding surface, and if any deviation occurs from the sliding surface, the controller will take respective action to bring the response to the line of the surface. However, with the SMC technique, the switching operation proceeds at discrete intervals of time which introduces chattering. To minimize this, fuzzy logic is implemented which compensates the deviation produced in SMC with its rule base and provides system stability. A comparative analysis is carried out with the fuzzy and SMC techniques as tabulated in Table 5.

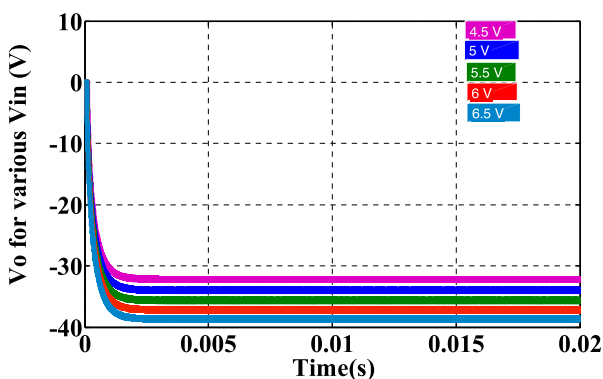
It is clearly shown that the fuzzy SMC shows better results than the conventional fuzzy technique in terms of the following.

- (1) The settling time ( $t_s$ ) of the response in fuzzy is 0.004 s whereas in Fuzzy SMC it settles at 0.001 s.
- (2) The delay time ( $t_d$ ) and rise time ( $t_r$ ) are 0.0001 and 0.001 s for fuzzy control and 0.00006 and 0.0009 s for SMC whereas it is about 0.00005 and 0.0001 s in FSMC control which is comparatively low when compared with SMC and fuzzy.
- (3) The output voltage is  $-35.45$  V in fuzzy and there is an increased output of  $-35.57$  V in FSMC control.

### 5.1. Simulation results of the FSMC-fed MNOSLC – line regulation

MNOSLC circuit is simulated for different values of input voltages and the response curve is plotted, as shown in Figure 16.

FSMC technique introduced in MNOSLC has conveyed the concept of line regulation. The simulation is

**Figure 16.** Line regulation plots of MNOSLC using FSMC.

carried out for 4.5, 5, 5.5, 6 and 6.5 V. It shows that the output lies between the range of  $-33$  and  $-37$  V. This shows that for variation in input, the output is maintained between the respective regulated limit values.

### 5.2. Simulation results of MNOSLC-fed FSMC – load regulation

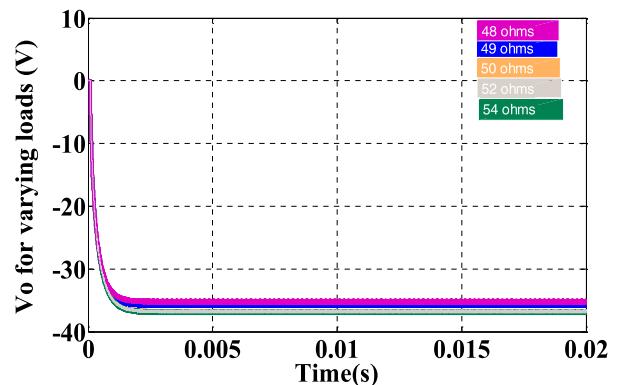
The regulation of the output voltage across the load is depicted in this section. The maintenance of standard DC magnitude for varying loads is shown here.

Figure 17 depicts the load regulation of MNOSLC using CMC-based FSMC control. It shows the magnitude of  $-35.33$  V for the ohmic value of  $48\Omega$  and the variation goes to  $-35.82$  for  $49\Omega$ . The output voltage magnitude has been depicted for 50 and  $52\Omega$  as  $-36.62$  and  $-36.79$  V. It also clearly shows a magnitude of  $-36.89$  V for 54. This conveys that the regulation of the voltage is maintained around  $-36$  V which satisfies the property of the controller. Thus, the load regulation is also achieved properly.

### 5.3. Hardware results of FSMC-fed NOSLC – line regulation

A prototype developed for MNOSLC is depicted in Figure 18. It shows the implementation of the PIC 16F877A microcontroller, driver IR2101 and the converter. The PIC controller projects the function of FSMC clearly to get the regulated output and the switching duty ratio which is maintained due to its performance. MNOSLC also depicts the rise of output for the input voltage applied.

The line regulation has been explained with the concept of maintaining the regulated output around  $-36$  V for different values of input voltages. Here it is depicted for two input voltages of 4.8 and 6 V, as shown in Figure 19. For 4.8 V, it shows an output of  $-34.6$  and for 6 V, it shows an output of  $-36.4$  V. The geometric progression is shown in the proposed value of 6 V with an output magnitude of  $-36.4$  V.

**Figure 17.**  $V_o$  (V) for variable loads.

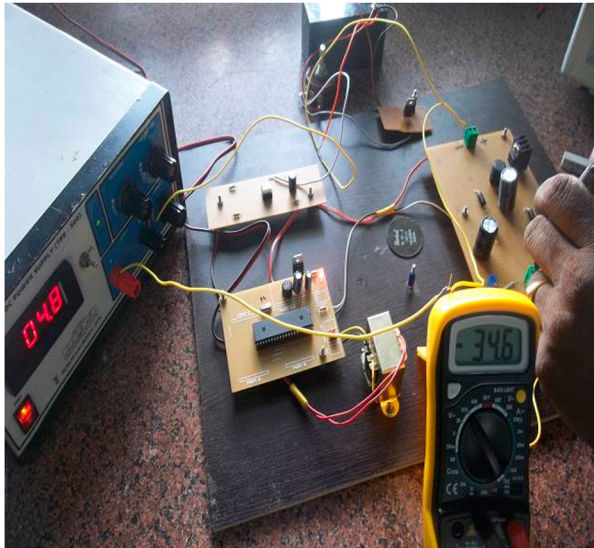


**Figure 18.** Overall Hardware of MNOSLC  $V_{in}$  of 4.8 V with  $V_{out}$  of  $-34.6$  V.

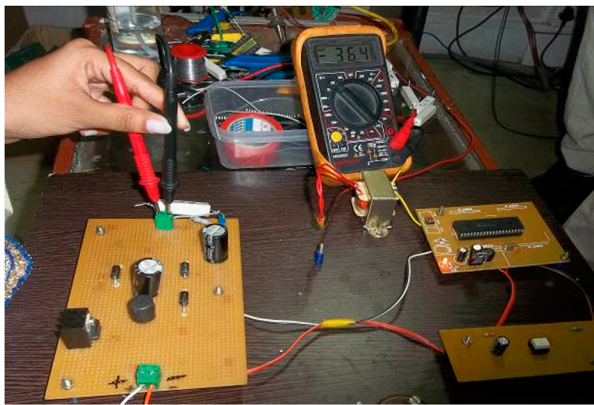


**Figure 19.**  $V_{in}$  of 6 V with  $V_{out}$  of  $-36.4$  V.

#### 5.4. Hardware results of MNOSLC-fed FMSC – load regulation

The hardware results of load regulation are depicted in this section. The voltage across the load is measured for varying loads and the constant level maintenance is depicted, thereby influencing the process of load regulation using CMC-based FSMC control.

The regulation at the load side is depicted in the figures. Figure 20 shows the output voltage of  $-36.6$  V for a load of 2 K. For the value of 1 K load, Figure 21 shows the output voltage of  $-35.8$  V. One important feature is the regulation which is again maintained around  $-36$  V even at the load side. Thus, the proposed concept is verified and validated at the source and the load side.

Chattering is defined as the oscillations in the control output that result in instability. SMC technique introduces this kind of chattering which is overcome in fuzzy-based SMC. Tuning the rule base of fuzzy makes the system travel on the sliding surface “S” in the FSMC technique and provides stability to the system. To overcome the chattering, the fuzzy technique

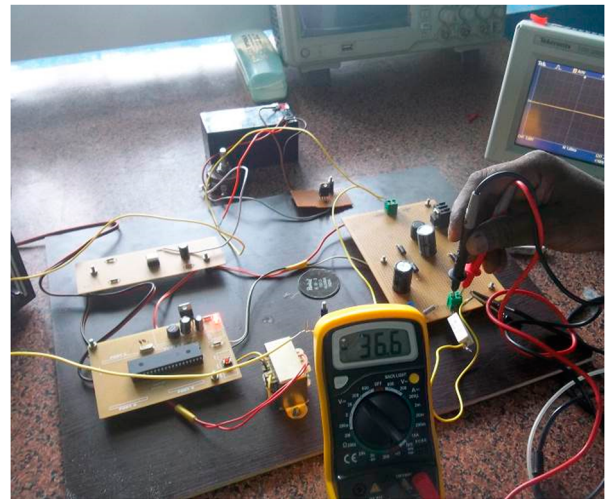


**Figure 20.**  $V_o$  of  $-36.6$  V for 2 K load.

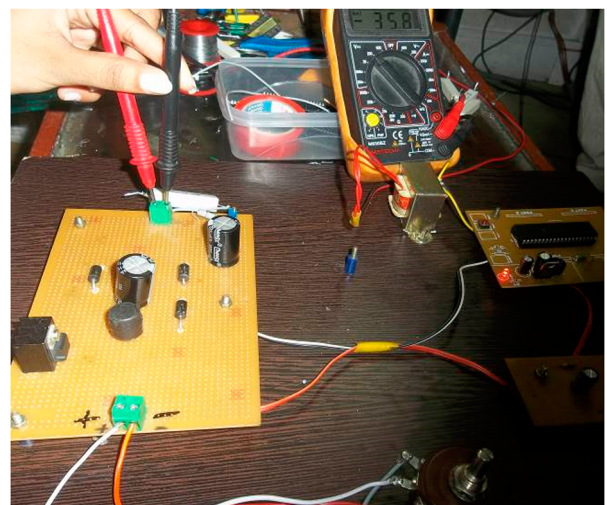


**Figure 21.**  $V_o$  of  $-35.8$  V for 1 K load.

is implemented as a method handler which is considered a non-conventional robust control. It is suitable for non-linear control a system that is characterized by parametric fluctuations.

Although a Fuzzy sliding mode controller is used to control partly unknown non-linear dynamic parameters of the non-linear system and the chattering effect without losing robustness against inaccuracies and varying loads, there exist some weak points and borders of the FSMC technique which are given as follows.

#### 5.5. Reaching phase

From the initial to the reach of the sliding surface is called the reaching point. It is tuned only by the controller and carried out by trial and error method. In this, the fuzzy rule base makes the response travel on the sliding surface.

The weak and the border points have been proposed for external load disturbance and found that the fuzzy tuning in SMC gives a better response for the load

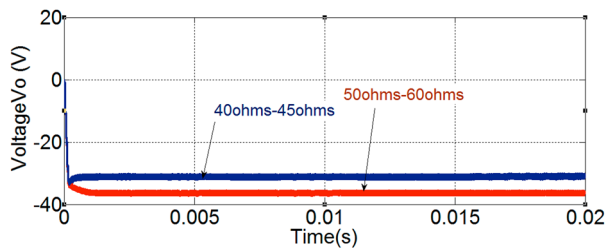


**Figure 22.** Output voltage ( $V_o$ ) of MNOSLC using FSMC for the variation in the load.

disturbance between 50 and 60  $\Omega$  when compared to a range between 40 and 45  $\Omega$  for an input of 6 V, as shown in Figure 22. It gives an output around  $-35$  V for the load values ranging between 50 and 60 ohms, whereas it gives an output of  $-31$  V for the other values of load.

## 6. Conclusion

This work has given the detailed analysis of different controllers employed for line and load regulation in MNOSLC circuits. The controllers portrayed are PI, fuzzy and SMC. The response of the PI controller has been shown only for the linear region of operation, as well as the output voltage ripple is found high, so, the non-linearity focus has been depicted through the implementation of a fuzzy controller. The expert knowledge concept is shown through the fuzzy rule base. The slow approach using fuzzy is compensated by the introduction of a sliding mode controller. The sliding coefficient selection for the generation of an energizing pulse has been portrayed. Although SMC has been shown in a better way than the conventional, the existence of duty cycle oscillation in this technique has been depicted. To compensate for these uncertainties, the implementation of FSMC has shown itself as a good dynamic controller with low ripple and steady-state output. Thus, the reference signal generation through FSMC has been conveyed for the current mode control. CMC has shown the line regulation through the comparison of inductor current with its reference magnitude and generation of exact duty cycle pulse to get a steady-state output. The effect of chattering and the weak points of FSMC are also explained.

## Disclosure statement

No potential conflict of interest was reported by the author(s).

## References

- [1] Cho BH, Bae HS, Lee JH. Review of current mode control schemes and introduction of a new digital current mode control method for the parallel module DC-DC converters. In: Power electronics and motion control conference. IEEE; 2009. p. 202–210.
- [2] Jang J, Pidaparthi SK, Choi B. Current mode control for LLC series resonant DC-to-DC converters. *Energies*. 2015;8:6098–6113. doi:10.3390/en8066098

- [3] Ramash Kumar K, Jeevananthan S. PI control for positive output elementary super lift Luo converter. *Int J Electric Comput Energetic Electron Commun Eng*. 2010;4(3):544–549.
- [4] Guo L, Hung JY, Nelms RM. Evaluation of DSP-based PID and fuzzy controllers for DC-DC converters. *IEEE Trans Ind Electron*. 2009;56(6):2237–2248. doi:10.1109/TIE.2009.2016955
- [5] Shtessel YB, Zinober AS, Shkolnikov IA. Sliding mode control of boost and buck-boost power converters using method of stable system centre. *Automatica*. 2003;39(6):1061–1067. doi:10.1016/S0005-1098(03)00068-2
- [6] Ramash kumar K, Jeevananthan K, Ramamurthy S. Improved performance of the positive output elementary split inductor-type boost converter using sliding mode controller plus fuzzy logic controller. *WSEAS Trans Syst Control*. 2014;9:215–228.
- [7] Silveira GC, Tofoli FL, Santos Bezerra LD, et al. A non-isolated DC-DC boost converter with high voltage gain and balanced output voltage. *IEEE Trans Ind Electron*. 2014;61(12):6739–6746. doi:10.1109/TIE.2014.2317136
- [8] Sheehan R. Understanding and applying current-mode control theory. Power electronics technology exhibition and conference; Dallas, TX; 2007.
- [9] Kiran N. Control of chaos in positive output Luo converter by means of time delay. *Int Electric Eng J*. 2015;6(2):1787–1791.
- [10] Sahraoui H, Drid S, Chrifi-Alaoui L, et al. Voltage control of DC-DC buck converter using second order sliding mode control. In: IEEE conference on control, engineering & information technology (CEIT); Algeria; 2015. p. 1–5.
- [11] Takahashi M, Deng M. Nonlinear robust power control of uncertain DC-DC converter with bilinear dynamics. *Global J Technol Optim*. 2014;6(1):1–5.
- [12] Allaoua B, Mebarki B, Laoufi A. A robust fuzzy sliding mode controller synthesis applied on boost DC-DC converter power supply for electric vehicle propulsion system. *Int J Vehicular Technol*. 2013;2013:1–9. doi:10.1155/2013/587687
- [13] Abdullah MA, Tan CW, Yatim AH, et al. Input current control of boost converters using current-mode controller integrated with linear quadratic regulator. *Int J Renew Energy Res*. 2012;2(2):262–268.
- [14] Jose J, Jayanand B. Simulation and implementation of superlift Luo converter. In: International conference on renewable energy and sustainable energy (ICRESE). IEEE; 2013. p. 128–132.
- [15] Bhowate A, Deogade S. Comparison of PID tuning techniques for closed loop controller of DC-DC boost converter. *Int J Adv Eng Technol*. 2015;8(1):2064–2073.
- [16] Muthukaruppasamy S, Abudhahir A. A indirect output voltage control in negative output elementary super lift Luo converter using PIC plus FLC in discontinuous conduction mode. *Circuits Syst*. 2016;7(11):434–444. doi:10.4236/cs.2016.711310
- [17] Khasawneh B, Sabra M, Zohdy MA. Paralleled DC-DC power converters sliding mode control with dual stages design. *J Power Energy Eng*. 2014;2(2):1–10. doi:10.4236/jpee.2014.22001
- [18] Soltanpour MR, Khooban MH, Khalghani MR. An optimal and intelligent control strategy for a class of nonlinear systems: adaptive fuzzy sliding mode. *J Vib Control*. 2016;22(1):159–175. doi:10.1177/1077546314526920

- [19] Kupati SK, Chavan M, Bhattad S, et al. Average current mode controlled power factor correction converter. *Indian J Sci Technol.* 2015;8(2):53–57. doi:10.17485/ijst/2015/v8iS2/60280
- [20] Reshma BR, Mathew AS. Gain scheduling implementation in DC/DC buck converter using PID controller. *Int J Eng Res Technol.* 2015;4(7):1063–1067.
- [21] Renwal D, Kumar M. Hybrid PI-fuzzy logic controller based DC-DC converter. In: International conference on green computing and internet of things (ICGCIoT); 2015. p. 753–757.
- [22] Sung HC, Park JB, Joo YH, et al. Robust digital implementation of fuzzy control for uncertain systems and its application to active magnetic bearing system. *Int J Control Automation Syst.* 2012;10(3):603–612. doi:10.1007/s12555-012-0318-4
- [23] Ilyas A, Jahan S, Ayyub M. Tuning of conventional PID and fuzzy logic controller using different defuzzification techniques. *Int J Scientific Technol Res.* 2013;2(1):138–142.
- [24] Su X, Shi P, Wu L, et al. A novel control design on discrete-time Takagi-Sugeno fuzzy systems with time-varying delays. *IEEE Trans Fuzzy Syst.* 2013;21(4):655–671. doi:10.1109/TFUZZ.2012.2226941
- [25] Anand R, Gnanambal I, Poornema N. Implementation of fuzzy logic controller for buck-boost converter combining ky and synchronous buck converter for battery operated portable devices. *J Theoret Appl Inf Technol.* 2014;67(1):151–158.
- [26] Shabanipoor M, Khajezadeh A, Zayandehroodi H, et al. Sliding mode control and stability analysis of a DC-DC converter buck. *BEPLS.* 2014;3(9):42–49.
- [27] Yang Y, Wang W, Zhou T. Sliding mode control based on three-sliding-surface for an inverted pendulum system. In: 33rd Chinese control conference (CCC); 2014. p. 65–70.
- [28] Etxeberria A, Vechiu I, Camblong H, et al. Comparison of sliding mode and PI control of a hybrid energy storage system in a microgrid application. *Energy Proc.* 2011;12:966–974. doi:10.1016/j.egypro.2011.10.127
- [29] Sahbani A, Ben Saad K, Benrejeb M. Fuzzy sliding mode control for parallel DC-DC boost converter. *Int Rev Electric Eng.* 2014;9(2):249–254.
- [30] Sahbani A, Ben Saad K, Benrejeb M. Chattering phenomenon suppression of buck boost dc-dc converter with fuzzy sliding modes control. *Int J Electric Electron Eng.* 2010;4(1):1–6.
- [31] Alaayed I, Bahja HE, Vega P. A sliding mode based on fuzzy logic control for photovoltaic power system using DC-DC boost converter. In: International conference on systems and control; 2013. pp. 320–325.
- [32] Chen B, Niu Y, Jia T. Sliding mode control for T-S fuzzy stochastic systems with markovian switching. In: 33rd Chinese control conference (CCC); 2014. pp. 49–54.
- [33] Fang W, Liu X-D, Liu S-C, et al. A digital parallel current-mode control algorithm for DC-DC converters. *IEEE Trans Ind Inf.* 2014;10(4):2146–2153. doi:10.1109/TII.2014.2358455
- [34] Bryant B, Kazimierczuk MK. Modeling closed-current loop of PWM boost DC-DC converters operating in CCM with peak current-mode control. *IEEE Trans Circuits Syst.* 2012;52:2404–2412. doi:10.1109/TCSI.2005.853904
- [35] Leppaaho J, Suntio T. Characterizing the dynamics of the peak-current-mode-controlled buck-power-stage converter in photovoltaic applications. *IEEE Trans Power Electron.* 2014;29(7):3840–3847. doi:10.1109/TPEL.2013.2281078
- [36] Li R, O'Brien T, Lee J, et al. Adaptive voltage positioning with average current mode control. In: IEEE energy conversion congress and exposition; 2013. p. 4961–4968.